INTERNATIONAL JOURNAL OF HYDROGEN ENERGY 46 (2021) 17751–17762

Available online at www.sciencedirect.com

ScienceDirect

journal homepage: www.elsevier.com/locate/he

# One-Step synthesis of $PtFe/CeO_2$ catalyst for the Co-Preferential oxidation reaction at low temperatures

*Rodolfo M. Antoniassi* [a,*], *Arthur P. Machado* [b], *Ana Rita N. Paiva* [b], *Carla M.S. Queiroz* [b], *Jorge M. Vaz* [b], *Estevam V. Spinacé* [b], *Julio Cesar M. Silva* [c], *Eduardo Carmine* [a], *Pedro H.C. Camargo* [a,d], *Roberto M. Torresi* [a]

[a] *Instituto de Química, Universidade de São Paulo, Av. Prof. Lineu Prestes, 748, Cidade Universitária, 05508-000, São Paulo, SP, Brazil*

[b] *Instituto de Pesquisas Energéticas e Nucleares – IPEN-CNEN/SP, Av. Prof. Lineu Prestes, 2242, Cidade Universitária, 05508-900 São Paulo, SP, Brazil*

[c] *Instituto de Química da Universidade Federal Fluminense, Grupo de Eletroquímica e Materiais Nanoestruturados, Campus Valonguinho, Niterói, RJ CEP, 24020-141, Brazil*

[d] *Department of Chemistry, University of Helsinki, A.I. Virtasen Aukio 1, Helsinki, Finland*

## HIGHLIGHTS

- Highly active Pt20Fe/CeO2 synthesized by borohydride without any pre-treatment.
- Fe species promotes the oxygen activation at low temperatures.
- $Pt_{20}Fe/CeO_2$ performance fulfills the CO-PROX "50:50 goal".

## GRAPHICAL ABSTRACT

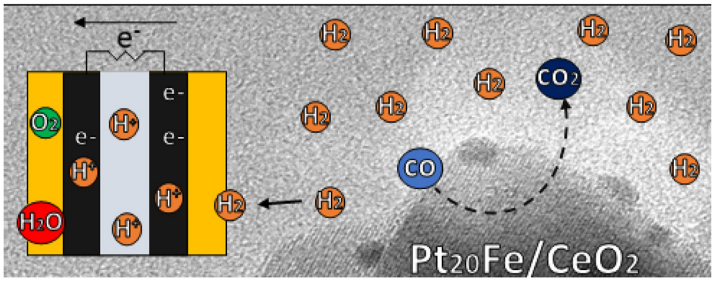


## ARTICLE INFO

*Article history:*
Received 12 September 2020
Received in revised form
14 January 2021
Accepted 24 February 2021
Available online 2 April 2021

*Keywords:*
Pt nanoparticles

## ABSTRACT

Active Pt-based catalysts at low temperature towards the preferential oxidation of carbon monoxide in hydrogen-rich stream reaction (CO-PROX) are of great importance for $H_2$-fueled fuel cells, but still remain a challenge. Herein, we propose a simple approach to synthesize a highly active $Pt_{20}Fe/CeO_2$ catalyst employing the borohydride reduction process. Transmission electronic microscopy revealed monodispersed 2.8 nm-Pt nanoparticles on $CeO_2$, and the role of Fe species on the activity is discussed. The excellent CO conversion of 99.6% and $CO_2$ selectivity of 92.3% carried out at ambient temperature meet the CO-PROX requirements for an adequate supply of hydrogen in fuel cell device.

* *Corresponding author.*
E-mail addresses: aidide@hotmail.com, aidide@usp.br (R.M. Antoniassi).

https://doi.org/10.1016/j.ijhydene.2021.02.192

Pt/Fe-based catalysts
CO-PROX
Hydrogen
Borohydride reduction process



## 1. Introduction

Hydrogen gas ($H_2$) is used in many essential processes, including petroleum cracking, methanol, fatty acids syntheses, and ammonia-based fertilizers. Recently, the *Hydrogen Economy* arose as one of the most desirable power supply alternatives for plenty of applications through Fuel Cell (FC) technologies fed by $H_2$ [1–7]. The possibility to obtain electricity from the cleaner combustion of the $H_2$ vector has motivated the development of efficient FC catalysts [8,9]. Hydrogen is mainly produced from the combined process of reform of natural gas and water-gas shift (WGS), yielding a $H_2$-rich mixture, which comprises $CO_2$ (about 10–20%), water (5–10%), and CO (1–5%). However, an extra purifying step is needed, since CO levels >100 ppm are not tolerated for appropriate catalytic performances [10]. Compared to the traditional techniques, chemical approaches like (photo) electrochemical water splitting [11–14] and the preferential oxidation of carbon monoxide in a hydrogen-rich stream in the presence of oxygen (CO-PROX) take valuable advantages of low-cost and environmentally friendly systems to produce hydrogen. CO-PROX is a suitable technique of purification, in which the presence of an active catalyst leads to a reacted $H_2$ stream containing acceptable CO levels [15]. To match the functional FC requests properly, there is an established benchmark for the CO-PROX reaction, which consists in reducing the CO concentration in at least 50 ppm with selectivity higher than 50%, currently so-called "50:50 Goal" [16].

Numerous efforts have been proposed on the development of supported platinum catalysts [10,17–21], because they are stable in CO-PROX reactor conditions over a range of temperatures (60–150 °C) [10] and also represent the state-of-the-art low-temperature FC catalysts. Besides, Pt would enable a coupled operating system without serious problems related to catalytic incompatibility. For these materials, physicochemical properties like size and composition/structure of the active/support phases play fundamental rules on the search for better CO-PROX catalysts [22–25]. The introduction of $CeO_2$ has remarkable importance on catalysis due to the oxygen mobility through its $Ce^{+3}/Ce^{+4}$ sites into the crystalline structure [26], which could favor oxidation reactions involving Pt–CO. However, even after six decades of cumulative reports, a very small number of examples can fulfill the 50:50 Goal, especially at low temperatures (<40 °C). These are the conditions at which stationary, automotive, and mobile FC-fueled devices usually start. This occurs as a result not only on insufficient activity related to poor CO conversion issues, but also of low $CO_2$ selectivity [21,27–38], resulting in the undesirable formation of water from the $H_2$ oxidation, thus compromising the quality of the $H_2$ outlet.

It is observed that PtFe-based materials are among the most active catalysts for CO-PROX reaction in the mild temperature range [28,32,34]. Some important contributions have shown that the addition of small amounts of Fe in the catalytic composition can substantially improve the CO-PROX activity [25,32,39,40]. The combined structure can both enhance the oxygen activation and weaken the strong CO adsorption on platinum through the modification of Pt d-band energy as a result of charge transfer centers. Thus, the introduction of Fe can benefit the catalytic performance at low temperatures, at which monometallic platinum is limited by CO poisoning [40]. Considering this composition, the optimum temperature at which higher conversion and selectivity occurs is ruled by different catalytic proprieties, which is obviously affected by the synthesis procedures. Most of the approaches employed are restricted to traditional methods, such as impregnation and microemulsion [21,27,29,31,32,38,41]. To achieve better performances, extra post-synthesis procedures are often adopted prior to introducing catalysts in the CO-PROX reactor, requiring, for example, determined conditions of synthesis media/washing and controlled heating or atmosphere treatments (or both combined in most cases). Such additional steps and chemicals not only extend time and expenses for the catalyst preparation but can also result in procedures that are difficult to reproduce. In this context, the sodium borohydride reduction process is a strong reducing agent, capable of reducing salts of noble metals to the zero valence through a fast kinetic, which is essential to form particles with controlled characteristics on the support. The process can also be conducted in a single step of reduction and deposition, enabling a synthesis procedure without any capping agents that may contaminate and perturb catalyst in the performance evaluation. According to previous studies, there are three independent reactions (equations (1)–(3)) that may play a role during the reduction of the cationic metal ($M^+$) in the presence of an aqueous solution of sodium borohydride [42]:

$$BH_4^- + 2H_2O \rightarrow BO_2^- + 4H^+ \quad (1)$$

$$nBH_4^- + 4M^{n+} + 2nH_2O \rightarrow 4\,M + nBO_2^- + 2nH_2 \quad (2)$$

$$BH_4^- + H_2O \rightarrow B + OH^- + 2.5H_2 \quad (3)$$

In addition, boron species could lead to a better dispersion of the nanoparticles on the support and decrease the size of the metallic particles, which is extremely advantageous to the catalytic performance [42]. The borohydride reduction process is a promising approach to produce other metals, especially for loadings <5%. Supported gold nanoparticles with small sizes (3–5 nm and loadings ranging from 0.5 to 2% could also

be prepared by similar approaches [43,44]; on the other hand, > 20 nm Au nanoparticles were obtained if the reducing agent is simply replaced by ethylene glycol and temperature of 160 °C [45], thus resulting in both lower activity and selectivity. Unfortunately, this sodium borohydride reduction process is still scarce towards CO-PROX materials, and it opens up new possibilities in terms of producing unexplored multimetallic compositions. Inspired by this fact, we report herein a rapid and facile preparation of $Pt_{20}Fe/CeO_2$ catalyst via $NaBH_4$ reduction process, without any post-synthesis treatment towards the CO-PROX reaction. The proposed catalyst showed high activity and selectivity at temperatures as low as 20 °C.

## 2. Materials and methods

All materials were used as received: hexachloroplatinic (IV) acid hexahydrated ($H_2PtCl_6 \cdot 6H_2O$, 99.9% purity, Sigma-Aldrich®), iron (III) chlorine hexahydrated ($FeCl_3 \cdot 6H_2O$, 97%, Sigma-Aldrich®), cerium oxide ($CeO_2$ nanopowder, <25 nm particle size (BET), Sigma–Aldrich®), sodium borohydride ($NaBH_4$, 98%, Sigma-Aldrich®), deionized water (18.2 MΩcm), $C_3H_7O$ (anhydrous isopropyl alcohol, 99.5%, Sigma-Aldrich®), $C_2H_6O_2$ (ethylene glycol, 99.5%, Vetec®).

Transmission Electronic Microscopy (TEM) images were collected on a JEOL equipment model JEM 2100F, operating at a voltage of 200 kV. Prior to TEM observation, all catalyst samples were dispersed in isopropyl alcohol, and sonicated for 10 min, and deposited on TEM copper grids. The sizes of the resulted nanoparticles were measured individually to construct the histograms. The energy-dispersive X-ray spectroscopy (EDS) was used to estimate semi-quantitatively the chemical composition of the catalysts by using a Philips scanning microscope (SEM - JEOL 1060, with electron source of 20 keV). To conduct the analysis, a small amount of the prepared catalytic powders was fixed in the carbon-coated sample holder. The atomic composition was verified by Inductively Coupled Plasma Optical Emission Spectroscopy (ICP-EOS). X-Ray Diffraction (XRD) were recorded by a Rigaku Miniflex II apparatus employing a Cu Kα source (λ = 1.54 Å). For XRD measurements, an aliquot of catalyst powder was deposited in a glass holder. To build the diffractograms, the information of $2\Theta = 20–90°$ was collected in a step size of 0.02° with an acquisition time of 1s. Hydrogen was used as a reducing gas for Temperature-Programmed Reduction (TPR) technique. The analyses were performed on ChemBET Pulsar TPR/TPD chemisorption instrument equipped with a thermal conductivity detector (TCD). To the analyses, an amount of 100 mg of each catalyst was inserted in a U-shaped quartz cell, and it was treated for 1 h under a nitrogen flow of 50 mL $min^{-1}$ at 200 °C. Then, all materials were let to cool to ambient temperature before being exposed to $H_2/N_2$ (10% $H_2$) flow (30 mL $min^{-1}$). The heating rate from ambient to 1000 °C was 10 °C $min^{-1}$.

### 2.1. Synthesis of 2.7 nm-$Pt/CeO_2$, $Fe/CeO_2$ and 2.8 nm-$Pt_{20}Fe/CeO_2$ catalysts

$Pt/CeO_2$, $Fe/CeO_2$, and $Pt_{20}Fe/CeO_2$ catalysts were prepared by a simple sodium borohydride reduction approach at ambient temperature (~20 °C). For $Pt/CeO_2$ synthesis, a beaker containing 495 mg of $CeO_2$, 25 mL of water, and 25 mL of isopropyl alcohol was sonicated to homogenize the cerium oxide support suspension for at least 10 min. After sonicated, the suspension was put under constant stirring, and 0.265 mL of an aqueous solution of $H_2PtCl_6 \cdot 6H_2O$ (0.05 g $mL^{-1}$) was quickly added. Then, 1 mL of an aqueous solution of sodium borohydride was introduced (6.5 mg $mL^{-1}$ - it was used an excess of the reducing agent in order to guarantee the complete reduction of metal precursor - $NaBH_4$:Pt about 6 in molar units). The catalyst was isolated and washed with water for 5 successively rounds of centrifugation at 8 k rpm. Finally, the material was dried at 80 °C for 2 h. A similar procedure was adopted for $Fe/CeO_2$ preparation, in which 2.43 mL of an ethylene glycol solution of $FeCl_3 \cdot 3H_2O$ (5 mg $mL^{-1}$) and 1 mL of sodium borohydride solution were added to the $CeO_2$ support suspension. For $Pt_{20}Fe/CeO_2$ synthesis, 0.24 mL of $H_2PtCl_6 \cdot 6H_2O$ was reduced with 1 mL of the $NaBH_4$ solution for 30 min in the same previous conditions. The material was isolated/washed and re-suspended in the isovolumetric water/isopropyl alcohol mixture prior to add 0.212 mL of the $FeCl_3 \cdot 6H_2O$ and 1 mL of $NaBH_4$. Then, those centrifugation and dry steps were repeated. The $Pt_{20}Fe$ nomenclature denotes the mass ratio between Pt and Fe phases, calculated by ICP.

### 2.2. Catalytic performance

The performance of the CO-PROX reaction was evaluated in a gas-phase system at atmospheric pressure, with 100 mg of each catalyst. The prepared materials were readily introduced in a fixed bed reactor without any pre-treatment prior to the performance measurements. The temperature of CO-PROX tests ranged from 20 to 150 °C in two subsequent cycles (runs) from the lower to higher temperatures, both at atmospheric pressure. The volumetric composition of inlet steam was 1% CO, 0.5% $O_2$, balanced with $H_2$, comprising 50 mL $min^{-1}$ of flow rate (weight hourly space velocity - WHSV = 30 L $g_{cat}^{-1}$ $h^{-1}$). The by-products and unreacted reagents were determined by Gas Chromatography (GC), coupled to the CO-PROX reactor. Prior to each catalyst performance, calibration curves were done to quantify CO, water, $CO_2$, and $O_2$. Both CO and $O_2$ conversions and $CO_2$ selectivity were calculated according to the following Equations (4)–(6):

$$\text{CO conversion (\%)} = 100 \cdot ([CO]_{in} - [CO]_{out})/(CO)_{in} \quad (4)$$

$$CO_2 \text{ selectivity (\%)} = 100 \cdot (0.5\,[CO_2]_{out})/([O_2]_{in}) - [O_2])_{out} \quad (5)$$

$$O_2 \text{ conversion (\%)} = 100 \cdot ([O_2]_{in} - [O_2]_{out})/(O_2)_{in} \quad (6)$$

For $CO_2$ selectivity, the coefficient 0.5 refers to the stoichiometric parameter, in which 1 mol of CO reacts to 0.5 mol of $O_2$, producing 1 mol of $CO_2$.

## 3. Results and discussion

The chemical reduction process involving the aqueous solution of sodium borohydride leads to a fast reduction of Pt (IV) ions into Pt (0) nanoparticles directly supported on $CeO_2$

through a single synthesis step. After the addition of sodium borohydride, the mixture color instantaneously changed from light yellow to grey, indicating the formation of platinum nanoparticles (PtNPs). The reaction rate is crucial to control the size and dispersion of the PtNPs in the absence of additional capping agents. TEM images are shown in Fig. 1. For $Pt/CeO_2$ (Fig. 1b and e), small PtNPs with a mean size of 2.7 nm (red histogram in FS 1a and Table 1) are observed on $CeO_2$ support. The interplanar distance of 2.3 Å corresponds to the (111) plane of PtNPs [46], whereas that of 3.1 Å is indexed to $CeO_2$ (111) [26] (Fig. 1e). PtNPs were found with good dispersion, and no regions of agglomeration were observed. Comparable observations were found for $Pt_{20}Fe/CeO_2$ (Fig. 1c and f), in which the average size of the PtNPs was 2.8 nm (green histogram in FS 1b). No visible Fe phases were observed for $Pt_{20}Fe/CeO_2$ (Fig. 1c and f) and $Fe/CeO_2$ (Fig. 1a and d), but the chemical analyses clarify its presence in the catalysts. The atomic composition of the catalysts evaluated by EDS is shown in Table 1. The Fe percentage for $Fe/CeO_2$ was 1.1%, and the Pt loadings of $Pt/CeO_2$ and $Pt_{20}Fe/CeO_2$ were found 1.44 and 1.39 wt %, respectively. The similar characteristics of loading and size found in the materials allow a more coherent evaluation of the compositional effect on the catalytic performance.

Iron was not detected in $Pt_{20}Fe/CeO_2$ sample, and this fact is attributed to the low content, thus limiting its quantification by EDS. ICP-EOS was employed to estimate the Pt and Fe contents of $Pt_{20}Fe/CeO_2$ exclusively. The wt. % results revealed that Fe corresponded to 0.07%, whereas Pt was found 1.44% (confirming both the platinum mass observed in EDS analysis and Pt:Fe ratio of about 20.6).

**Table 1 – Size and compositional characterization of the catalysts.**

| Catalyst | Nanoparticle size (nm) | EDS (wt. %) | | |
|---|---|---|---|---|
| | | Pt | Fe | $CeO_2$ |
| $Fe/CeO_2$ | – | – | 1.10 | 98.90 |
| $Pt/CeO_2$ | 2.7 | 1.44 | – | 98.56 |
| $Pt_{20}Fe/CeO_2$ | 2.8 | 1.39 | undetectable | 98.51 |

Fig. 2a depicts the X-ray diffractogram data of $Fe/CeO_2$, $Pt/CeO_2$ and $Pt_{20}Fe/CeO_2$. For comparison purposes, $CeO_2$ data were included. In all cases, characteristic peaks assigned to the cubic cerium oxide structure at approximately $2\Theta = 28.3°$, 33°, 47.4°, 56.2°, 59°, 69.3°, 76.5°, 79° and 88.3° (ICSD #72155) were observed. The thin peaks correspond to the crystalline $CeO_2$ structure of >25 nm. On the other hand, the peaks related to the Pt and Fe species are absent. This is associated with a small amount and/or low crystallinity of both species onto the $CeO_2$ support. To have information about Fe crystalline characteristics of the catalysts, the synthetic procedure was reproduced in the absence of the Pt precursor and $CeO_2$. The synthesis recipe was proportionally multiplied by a factor of 5 in order to collect enough amount of sample. Then, part of the obtained material was dried at 80 °C, and then another one was submitted to 150 °C, which represents the temperature to dry the as-synthesized catalysts and the maximum

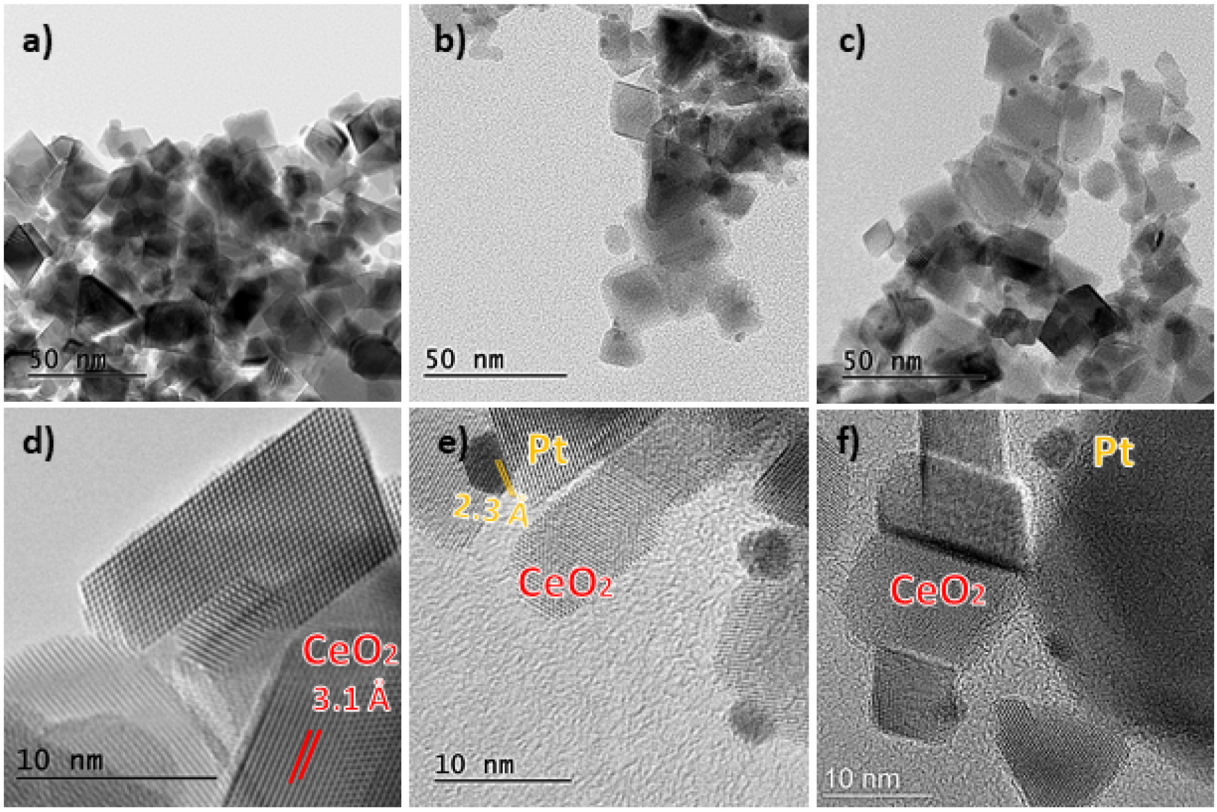


**Fig. 1 – TEM micrographs of $Fe/CeO_2$ (a, d), $Pt/CeO_2$ (b, e) and $Pt_{20}Fe/CeO_2$ (c, f).**

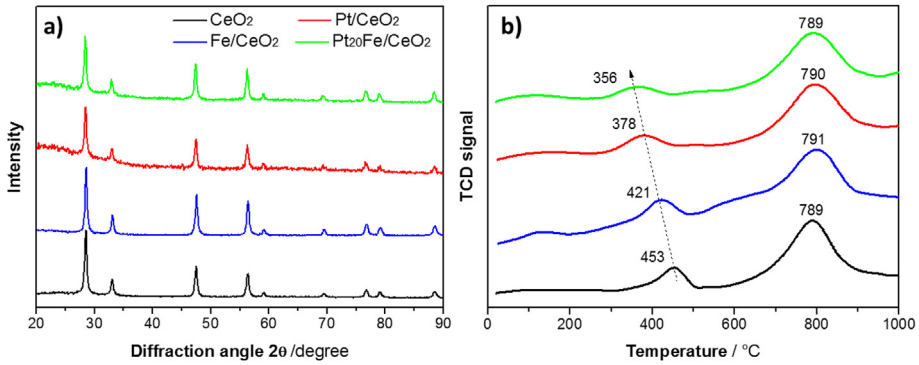


**Fig. 2 – a) X-ray diffraction data and b) $H_2$-Temperature programmed reduction of $CeO_2$ supported $Fe/CeO_2$, $Pt/CeO_2$ and $Pt_{20}Fe/CeO_2$.**

temperature in CO-PROX experiments. The XRD measurements of both materials revealed an amorphous behavior (FS 1c), which suggests that the Fe is dispersed on the catalysts as an oxide/hydroxide phase.

Fig. 2b shows the $H_2$-TPR analysis for $CeO_2$, $Fe/CeO_2$, $Pt/CeO_2$ and $Pt_{20}Fe/CeO_2$. In all profiles, there are two regions of hydrogen consumption regarding the reducion of different species; one in the range of 300–600 °C and the second at temperatures above 600 °C. Harrison et al. [47] reported a pair of reduction peaks for $CeO_2$: the first at 500 °C, assigned to the reduction of the surface species and the other one at 800 °C, corresponding to the reduction of bulk oxygen and the formation of lower oxides of cerium. For the commercial $CeO_2$ support, this pair of peaks is centered at 453 °C and 789 °C, respectively. There were no changes in the peak position related to the bulk $CeO_2$ for all materials, apparently. Conversely, the peaks related to the Ce surface sites shifted towards lower temperatures for all the synthesized materials. Such features are typical for deposited particles on $CeO_2$ supports [48,49]. In the case of $Fe/CeO_2$, it appeared at 421 °C. Although Fe species cannot be identified in TEM images nor by XRD, it is evidenced that the surface sites of Ce were modified as a function of the Fe deposition. For $Pt/CeO_2$, the first peak was displaced at 378 °C, whereas for $Pt_{20}Fe/CeO_2$, this value is almost 100 °C lower than that of the commercial $CeO_2$. Taking to account the Pt loading is virtually the same in $Pt/CeO_2$ and $Pt_{20}Fe/CeO_2$, the displacement in the TPR curves cannot be related to the platinum load but to the Fe deposition. Besides, it is presumed that the Fe is well dispersed, presenting an intimate contact with Pt and $CeO_2$; otherwise, no displacement would be expected, considering the very low amount of Fe in $Pt_{20}Fe/CeO_2$. The deposition of Pt and Fe via sodium borohydride suggests that these species could bond directly on $CeO_2$, thus changing the reduction temperature related to the Ce surface sites. The shift towards lower temperatures may indicate a metal-support interaction, which could enhance the oxygen mobility through the $CeO_2$ cubic lattice, thus leading to the improvement of the redox properties of the catalysts [49,50]. Thus, these results indicate that Fe, Pt, and $Pt_{20}Fe$ species promote an interface interaction with $CeO_2$ support.

Fig. 3 shows the CO-PROX performances of $Fe/CeO_2$, $Pt/CeO_2$ and $Pt_{20}Fe/CeO_2$ with $\lambda = 1$ (inlet feed ratio of $O_2$/CO = 0.5), following the operational conditions of a previous report [49]. There was no pre-treatment prior to the catalytic CO-PROX experiments, and the materials were tested just as synthesized. Three chromatographic runs were conducted for each temperature, and the results represent the mean values with error bars. Here, the second run was reported for each material. After the first run (going from 20 to 150 °C), the samples were let to cool naturally until 20 °C inside the reactor prior to starting the second run. Generally, the samples were more active in the second run, performing better, especially at temperatures up to 75 °C. This fact may be related to the decrease of the cationic species during the first run, thus improving the accessibility of the gas feed through the active sites. For temperatures >75 °C, both first and second runs performed similarly. From Fig. 3a, it is verified that the combination of Fe species with $CeO_2$ support is not a good choice to activate the CO oxidation, at least at the conditions studied. $Fe/CeO_2$ did not provide a significant catalytic response, and about 2% of CO conversion was observed at 20 °C, with 12% of $CO_2$ selectivity. The performance practically does not change at higher temperatures with the maximum of CO conversion of 3% and 17% of $CO_2$ selectivity at 150 °C. The $O_2$ consumption is shown in Fig. 3d (blue line). Low quantities of oxygen were consumed in the range of 20–150 °C (about 15%). Considering the low conversions of CO and $O_2$, together with unreacted $H_2$ outlet, one could infer that or $Fe/CeO_2$ are unable to adsorb both CO and $H_2$ (or it can be done in very small portions) or the material surface is quickly covered by CO in the temperatures studied. Both CO conversion and $CO_2$ selectivity curves obey a volcano-type profile for $Pt/CeO_2$, indicating a limitation in the CO-PROX performance at ambient temperature. In such conditions, the CO conversion is very poor (6% of conversion and 27% of $CO_2$ selectivity). However, the CO conversion increases with the temperature increasing up to 75 °C. This behavior was already expected since carbon monoxide strongly blocks platinum sites at lower temperatures, thus hampering the oxygen adsorption (see the low $O_2$ conversion at 20 °C – Fig. 3d, red line). Hence, based-platinum materials are typically inactive at ambient temperatures [29,51,52]. The interaction of Pt–CO weakens as the temperature increases, and then oxygen and carbon monoxide can compete onto platinum sites. The proximity of these adsorbates on $Pt/CeO_2$ promotes the increase of $CO_2$ formation, releasing occupied

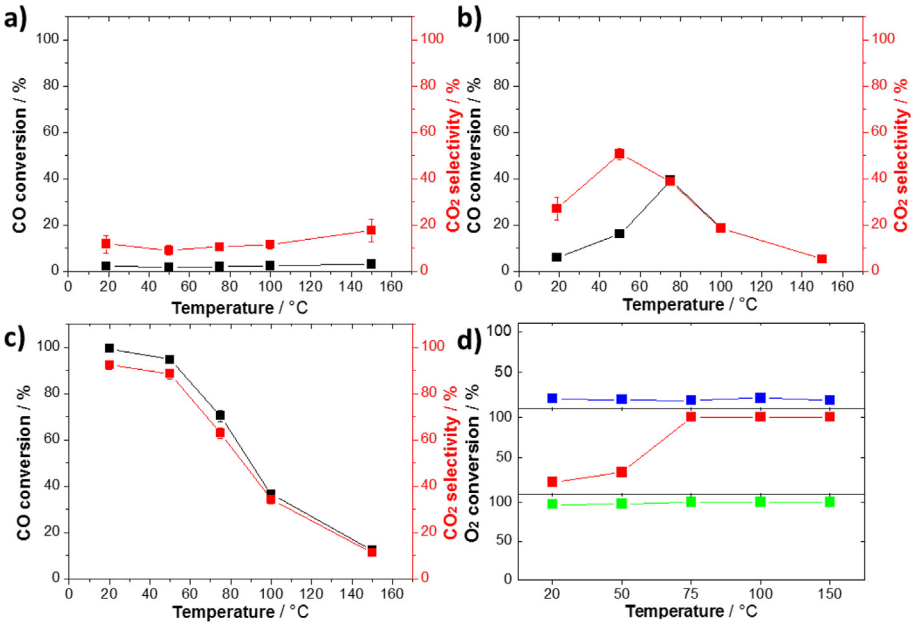


**Fig. 3 – CO-PROX reaction performance of a) $Fe/CeO_2$, b) $Pt/CeO_2$, c) $PtFe/CeO_2$ and d) $O_2$ conversion for $Fe/CeO_2$ (blue line), $Pt/CeO_2$ (red line) and $Pt_{20}Fe/CeO_2$ (green line). (For interpretation of the references to color in this figure legend, the reader is referred to the Web version of this article.)**

sites for subsequent adsorption processes. At 75 °C, the maximum conversion was about 40% with almost 40% of $CO_2$ selectivity. In higher temperatures, CO desorption occurs, and hydrogen adsorption can take place, resulting in a drop of the CO conversion. Consequently, the $CO_2$ selectivity decreases because of the formation of water by hydrogen oxidation. This situation is evidenced by the $O_2$ conversion, which maintained 100% in temperatures above 75 °C. Surprisingly, $Pt_{20}Fe/CeO_2$ behaves quite differently. It is interesting to note that, although structural details of the obtained Fe species missed in TEM and XRD analyses, the CO-PROX activity by itself is an elegant evidence that not only relates the Pt and Fe presence in the catalyst, but also demonstrate their intimal contact on $CeO_2$ support - as also found in $H_2$-TPR and ICP data. More importantly, such a synergetic combination is beneficial for CO-PROX performance at ambient temperature, providing a significant improvement compared to the $Fe/CeO_2$ and $Pt/CeO_2$ limited counterparts. The CO conversion is about 99.6%, with 92.3% of $CO_2$ selectivity. At 50 °C, the CO conversion slightly decreases to 95% with about 89% of $CO_2$ selectivity. Unlike most PtFe-based reported materials (see Table 2), the $Pt_{20}Fe/CeO_2$ was very active at low temperatures. At temperature higher than 75 °C, the activity drops to 70% of conversion and 63% of selectivity. This behavior is frequently verified in other reports [23,35]. It is worth mentioning that $Pt_{20}Fe/CeO_2$ is not limited by the oxygen activation in lower temperatures, as observed for $Pt/CeO_2$ and $Fe/CeO_2$ catalysts. Thus, oxygen consumption needed to achieve satisfactory conversions in lower temperatures can avoid the complete CO blockage (Fig. 3d). The hydrogen oxidation also took place at temperatures higher than 75 °C; however, $Pt_{20}Fe/CeO_2$ is 75% more active than $Pt/CeO_2$ and 68% more selective to $CO_2$, with similar $O_2$ conversions. This means that the addition of small amounts of Fe species not only drives structural modifications that improve the Pt–CO interaction at higher temperatures compared to $Pt/CeO_2$, but it also provides a scenario that matches the 50:50 fuel cell requests in CO-PROX reaction at 20 °C. Two other factors may have also contributed mutually to the excellent $Pt_{20}Fe/CeO_2$ performance: the metal-support interaction and size of the nanoparticles. For Gatla et al. [22] the amount of oxygen vacancies is increased for $CeO_2$ at a nanosized level. They reported an elongated Pt–O bond distance in the Pt–O–Ce link of PtNPs (of about 1 nm) dispersed on nanosized $CeO_2$, resulting in easily removable oxygen, which could be extremely desirable for CO oxidation at low temperatures. For Ganzler et al. [53], the interface of Pt and $CeO_2$ sites can be tuned by controlling the size of the PtNPs. They demonstrated that Pt particles up to 2 nm not only induced modifications in the reducibility characteristics of $CeO_2$ but also provided an intimate interaction with the oxide, which can activate the redox chemistry and enhance the low-temperature CO oxidation reaction.

To contextualize $Pt_{20}Fe/CeO_2$ proposed herein, we highlight synthesis details, and the catalytic performance of the most efficient PtFe materials for CO-PROX reaction reported up to date. It is important to point out the difficulty in establishing proper comparisons since structural/composition characteristics of the materials [24,25,32] and the operational conditions at which CO-PROX reacts (such as inlet composition [24], λ and WHSV [23] dramatically affect the performance). Importantly, the last two variables can even distinguish whether or not the material fulfills the 50:50 Goal, in such a way that higher conversions at lower temperatures are found for lesser WHSV and higher λ [23]. The most notorious CO-PROX performances have pointed out that the Pt:Fe ratio is regulated higher than 1 or even employ Fe in trace levels [25,32,35,39,40]. Table 2 shows materials synthesized by different approaches, in which several Pt:Fe ratios are

**Table 2 – Comparison of the catalytic performance of PtFe-based materials for CO-PROX reaction reported in the literature.**

| Method | Catalyst composition | Pt loading (%) | Catalyst treatment process before reaction | Particle size (nm) | Feed composition (vol %) | Space velocity | $O_2$/CO ratio | $T_{max}$[a] (°C) | CO conversion (%) | $CO_2$ selectivity (%) | Ref. |
|---|---|---|---|---|---|---|---|---|---|---|---|
| Microemulsion | $Pt@Fe_3O_4@SiO_2$ | 4 | calcined at 550 °C for 2 h | 20 | 1.5% CO, 0.75% $O_2$, 80% $H_2$ and $N_2$ | – | 0.5 | 100 | 51 | 60 | [27] |
| Impregnation $[(C_4H_9)_4N]_2[Pt_3(CO)_6]_n$ | Pt/γ-$Fe_2O_3$ PtCO/γ-$Fe_2O_3$ | 2–4 | heating from 30 to 200 °C, 40 min of isothermal at 200 °C and cooling until 60 °C | 1.8 | 70–50% $H_2$, 1–2% $O_2$, 1% CO, 0–15% $CO_2$, 0–5% $H_2O$ and He | 100 mL $min^{-1}$ | 2 | 87 | 80 | 86 | [21] |
| Incipient wetness impregnation | $Pt/Fe_3O_4$ | 5 | Calcinated at 300 °C | 2 | 0.5%CO, 0.5%$O_2$, 50%$H_2$ balanced with He | 50 $cm^3$ $min^{-1}$ | 1 | 80 | ~30 | – | [31] |
| Wet impregnation | $PtFe_x/C$ | 4 | 2 h with 5% $H_2$ at 400 °C | 1.8–2.3 | 1% CO, 0.5% $O_2$, 50% $H_2$ | 80 mL $g^{-1}$ $h^{-1}$ | 0.5 | 40 | 100 | ~40 | [32] |
| Flame spray pyrolysis | $Pt/Fe_2O_3$ | 5 | Treated with $H_2$/Ar at 200 °C for 1 h. | | 1% CO, 2% $O_2$, 88% $H_2$ in He | 7640 $h^{-1}$ | 2 | 100 | >90 | 20 | [33] |
| Calcination (800 °C) | $Pt/LaFeO_3$–$CeO_2$ | 0.5–5 | – | 29 | 1%CO, 1,5%$O_2$, 50% $H_2$ balanced with Ar | – | 3 | >100 | 99 | 95 | [34] |
| Deposition of Fe on Pt (111) | $FeO_x$/Pt (111)/$SiO_2$ | – | Annealing 200 °C in UVH | 2–4 | 1%CO, 0.5%$O_2$, and 98.5%$H_2$ | 36,000 mL $g^{-1}$ $h^{-1}$ | 0.5 | 80 | 95 | 95 | [35] |
| Ethylene glycol | Alloyed $PtFe_x/Al_2O_3$ | – | heating in a He and $H_2$ for 1 h at 400 °C | 1–4 | 2%CO + 40% $H_2$ + 1%$O_2$ balanced with He | 40,000 $cm^3$ $g^{-1}$ $h^{-1}$ | 0.5 | 140 | ~45 | 40 | [36] |
| Organometallic synthesis $Na_2Fe(CO)_4$ 3/2$C_4H_8O_2$ Pt (COD)$Cl_2$ | $Pt_5Fe_2/SiO_2$ | 1 | heated to 350 °C | 2 | 0.5%CO, 0.5%$O_2$, 45%$H_2$ balanced $N_2$ | 120 L $g^{-1}$ $h^{-1}$ | 1 | 140 | >90 | ~50 | [37] |
| Impregnation of Pt/$TiO_2$ in a $Fe(NO_3)_3$ solution | 1%$FeO_x$/1%$PtCeO_2$ | 1 | Calcined at 400 °C in air | – | 3%CO, 1.5%$O_2$, 20% $H_2$ balanced with $N_2$ | 100 mL $min^{-1}$ | 0.5 | >60 | 90 | ~80 | [38] |
| Ion-exchange ($[Pt(NH_3)_4]Cl_2$ and $Fe(NO_3)_3$) | Pt–Fe/mordenite | 0.5–4 | $N_2$/$O_2$ flow at 300 °C for 1 h, heated at 300 °C under $H_2$ | – | 1%CO, 0.5%$O_2$, and $H_2$ balance | 50,000 $h^{-1}$ | 1 | 50 | 90 | 95 | [28] |
| Impregnation of Pt/$Al_2O_3$ in a $Fe(NO_3)_3$ solution | 1%$FeO_x$/1%Pt/$Al_2O_3$ 100%$FeO_x$/1%Pt/$Al_2O_3$ | 1 | Calcined at 400 °C in air | – | CO, $H_2$, and $O_2$: 1.5:20:3 mL/$min^{-1}$ | 1470 mL $h^{-1}$ | 2 | 80 110 | ~40 ~30 | ~50 | [29] |

(continued on next page)

obs-

**Table 2 – (continued)**

| Method | Catalyst composition | Pt loading (%) | Catalyst treatment process before reaction | Particle size (nm) | Feed composition (vol %) | Space velocity | $O_2$/CO ratio | $T_{max}$ [a] (°C) | CO conversion (%) | $CO_2$ selectivity (%) | Ref. |
|---|---|---|---|---|---|---|---|---|---|---|---|
| Ion-exchange | Pt–Fe/Mordenite | 6 | $O_2$ at 500 °C for 0.5 h and $H_2$ at 500 °C for 1 h | 1 | 1.0% CO, 0.5% $O_2$ and $H_2$ balance. | 50 $cm^3$ $min^{-1}$ | 0.5 | 100 | 100 | 100 | [30] |
| impregnation | Fe–Pt/$Al_2O_3$ | 5 | calcined at 500 °C | – | $H_2$: 42%, $CO_2$: 9%, $H_2O$: 12%, CO: 0 –1.0%, $O_2$: 0–1.0% | 30,000 $h^{-1}$ | 1 | 100 | 80 | 40 | [41] |

[a] $T_{max}$: temperature of maximum CO conversion.

erved, mostly containing about 0.5–2% metallic loading, similar to the $Pt_{20}Fe$ content of the current catalyst. Employing the same operational conditions of this present study, we reported that Pt loadings up to 1% are also the best compositions for $Pt/CeO_2$ catalysts (prepared by ethylene glycol reducing agent, with the same support) in terms of CO conversion and $CO_2$ selectivity [49]. Lou et al. [40] synthesized $PtFe/\gamma\text{-}Al_2O_3$ catalyst by a multistep method through a modified adsorption approach by carefully pumping the precursor solutions to the support with a controlled speed rate and pH. Successive additional steps such as washing, drying, and thermal treatments in a controlled atmosphere were done before to CO-PROX reaction. Despite the complexity of the preparation, their catalyst showed efficient performance (100% of CO conversion and 50% of $O_2$ selectivity) at a range of temperature upon oxygen excess ($\lambda = 2$) and 50% of $H_2$ in He-balanced inlet condition (comprising one of the lowest values of WHSV, 20 L $h^{-1}$ $g^{-1}$). Fu et al. [35] proposed a high platinum-loaded Pt–Fe/$SiO_2$ catalyst (4% wt. Pt loading and 0.5% of Fe, though a modified sol-gel method), which also involved additional procedures of thermal and atmosphere treatments. They reported 100% of CO conversion at RT condition, $\lambda = 1$ and 36 L $g^{-1}$ $h^{-1}$, but a significant decrease in both conversion and selectivity was observed with the temperature increasing until 500 K. Through a thermal synthesis method, Zhang et al. [32] prepared a class of $PtFe_x/C$ catalysts (also comprising 4% wt. Platinum, but with different Fe compositions), combining ethylene glycol, temperature, inert atmosphere pressurization and pH assisted conditions during the synthesis steps. They reported CO conversion values around 100% at 40–50 °C (and at least 85% in the temperature range of 160 °C) employing one specific Pt/Fe atomic composition, $\lambda = 1$ and 80 L $g^{-1}$ $h^{-1}$. Lopez et al. [23] prepared 5% platinum loaded Pt–$Fe_3O_4/\alpha\text{-}Al_2O_3$ by a multistep thermal synthesis using a rotatory oven, atmosphere, pH, temperature and time conditions, and a range of chemicals. They found about 100% CO conversion at 20–40 °C with $\lambda = 2$ and 30 L $g^{-1}$ $h^{-1}$ and 70–80% in the stability test, achieving 40% of $CO_2$ selectivity under $\lambda = 2$ with the same WHSV stream. Cao et al. [39] reported the deposition of different Fe multilayers on selective Pt sites of $Pt/SiO_2$ through the sophisticated Atomic Layer Deposition (ALD) technique. Values of 100% in CO conversion and selectivity were found in a temperature range of 250–300 K, with WHSV varying from 36 to 288 L $g^{-1}$ $h^{-1}$ with 1% CO, 0.5% $O_2$, and 48% $H_2$ He-balanced feed.

We believe that these are the best Pt–Fe catalytic reports, which successfully overcome the 50:50 Goal for hydrogen purification at ambient conditions. In general, the successful ratio in CO-PROX catalysis is scarce, and it is notable that the highlighted materials depend on syntheses involving rather complex procedures and/or larger quantities of precious metal, demanding higher costs and time. On the other hand, the $Pt_{20}Fe/CeO_2$ produced by the simple borohydride strategy did not require many chemicals or post-synthesis treatment to achieve high performance in conditions at which the major of the Pt-based catalysts fail.

To study the stability of $Pt_{20}Fe/CeO_2$, the deactivation was monitored periodically in 100 consecutive tests during 27.5 h of uninterrupted observation. The stability was

conducted after the catalytic reactor bed cooled, reaching the temperature of 20 °C from the performance experiment of Fig. 3c. It is noted that CO conversion gradually decreased with stream time, and values of about 80% were observed at the end of the test (Fig. 4a). Despite the CO conversion drop, the $CO_2$ selectivity increased to 100%, and it was maintained after the third injection at 25 min of the stream time, in a way that the selectivity was not compromised by the CO conversion drop. The $O_2$ conversion (Fig. 4b) also decreased with the stream time, following the CO conversion trend. Lopez et al. [23] reported similar deactivation results for 4.9% wt Pt Pt–$Fe_3O_4$–$Al_2O_3$ during 25 h on stream, but it was conducted at 85 °C with 60 L $g^{-1}$ $h^{-1}$ instead of 25–50 °C and 30 L $g^{-1}$ $h^{-1}$ (conditions at which the best performance was found before the deactivation). They observed $CO_2$ selectivity values almost constant (around 40%) and CO conversion drop in the order of 10% (initially found in 80%) after 25 h at 85 °C with $\lambda = 2$. The deactivation reason was attributed to the adsorption of components likely from the $H_2$ oxidation at 85 °C after "regenerating" the deactivated sample by heating at 230 °C for 3 h. Indeed, as previously commented, the temperature increasing accelerates the competition between CO and $H_2$ for the Pt sites, thus facilitating the $H_2$ oxidation. However, the regeneration procedure did not fully restore the proprieties of the non-deactivated material since CO conversion decreased and $CO_2$ selectivity increased (approximately 5 and 25%, respectively) at temperatures < 40 °C, which may indicate that water formation is the imperative but not an exclusive reason for Pt–$Fe_3O_4$–$Al_2O_3$ deactivation. Considering our $CO_2$ selectivity results, the formation of water is not the main reason for deactivation. Besides, sintering effects and carbon deposition onto nanoparticles surface could also be unlikely causes, considering the temperature employed. Instead, it is reasonable to expect the oxygen present in the inlet causes gradual changes in the catalyst structure, thus leading to a slow deactivation. Zhang et al. [25] evaluated the deactivation of allowed $Pt_{0.71}Fe_{0.23}$ catalyst by submitting it to oxygen and CO treatments. They found a dramatic decrease in both CO and $O_2$ conversions after pre-treating the material with $O_2$, while small changes were observed after the CO pre-treatment in conditions of $\lambda = 2$ and WHSV = 20 L $g^{-1}$ $h^{-1}$. By comparing the untreated and pre-treated catalytic performances and quasi-in situ XPS data, the authors attributed that the deactivation was ruled by the oxidation of Fe species rather than Pt oxidation or poisoning. In addition, different amounts of $O_2$ were also tested without pre-treatments, and the relative deactivation was found more intense as λ increased during 7.5 h of stream time. Interestingly, for both untreated and pre-treated cases, higher CO conversion values were found compared to $O_2$ conversions, except for the case of $\lambda = 1$, but no related commentaries were drawn. By changing the support to $TiO_2$, the CO-PROX stability was improved. It is expected $TiO_2$ can better activate oxygen, thus maintaining the PtFe nanoalloy more stable than that in the case of $Al_2O_3$ substrate. It is important to point out that our material exhibited similar performances, although no alloy may be formed (since there was no treating step in the synthesis and the material was not submitted to temperatures higher than 150 °C in the CO-PROX experiment). This means that the combination of platinum with another Fe species are equally important for CO oxidation, such as evidenced by Ref. [39], in which monolayers of ionic Fe species that were ALD introduced on Pt sites of Pt/$SiO_2$ catalyst are responsible for boosting the CO oxidation. The authors also considered that Fe (OH)x species are inactive in the absence of Pt (as observed for our Fe/$CeO_2$ material), and the support can enable strong Pt–Fe (OH)x interactions that could provide stable sites for CO-PROX reaction. These contributions confirm the importance of an optimum interaction between Pt with Fe phases on the support interface for redox chemistry that involves the oxygen activation at low temperatures. In line with the literature [32,40,54–56], we trust that the improved performance of the $Pt_{20}Fe/CeO_2$ is attributed to the Pt and $FeO_x$ interaction, thus leading to a weakening of the interaction of CO at Pt sites and the activation of oxygen, especially on $FeO_x$ species at ambient temperature. On the other side, considering the stability tests of $Pt_{20}Fe/CeO_2$ and that of Pt/$CeO_2$ [49], one can assume that Fe species of $Pt_{20}Fe/CeO_2$ are the main responsible for the performance drop with time, given the same operating conditions and structural similarities of both materials. In this sense, it is highly acceptable for iron species to change, due to the oxygen in the inlet flow, then becoming species with a higher oxidation state, for example, from $Fe^{2+}$ to $Fe^{3+}$. $Fe^{2+}$ acts as actives sites for oxygen activation, whereas the same process is seriously hampered on $Fe^{3+}$ [25], decreasing the oxygen conversion ability. It is noted that although $Pt_{20}Fe/CeO_2$ had the $CO_2$ selectivity unaltered, the $O_2$ conversion has progressively decreased over time, thus leading to a gradual loss of

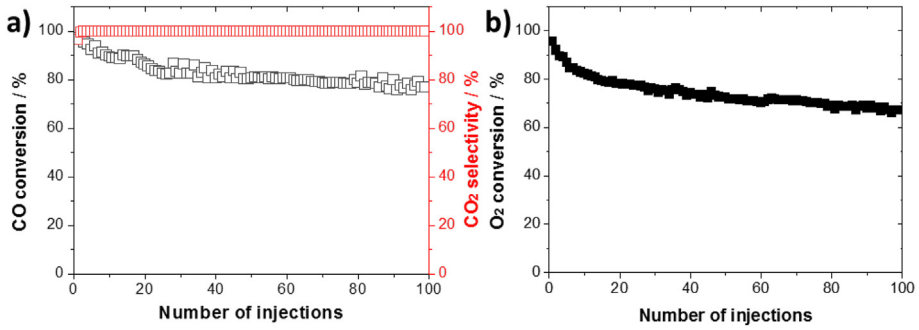


**Fig. 4 – Long-term performance of $Pt_{20}Fe/CeO_2$ along 100 consecutive reaction injections at 20 °C. a) CO conversion and $CO_2$ selectivity and b) $O_2$ conversion.**

performance during CO-PROX reaction, likely due to the formation of $Fe^{3+}$; however, further studies are needed to confirm this hypothesis.

## 4. Conclusions

$Fe/CeO_2$, $Pt/CeO_2$, and $Pt_{20}Fe/CeO_2$ were synthesized without any pre-treatments by a facile sodium borohydride approach and were applied for CO-PROX reaction. The obtained materials presented disperse PtNPs with size of 2.7 and 2.8 nm. The incorporation of a small amount of Fe in $Pt_{20}Fe/CeO_2$ catalyst resulted in high performance in terms of CO conversion and $CO_2$ selectivity at 20 °C. This performance could be attributed to the synergetic interaction between Pt and Fe with $CeO_2$ support, favoring the $O_2$ activation in low-temperature conditions in the $Pt_{20}Fe/CeO_2$ interface. More studies about the effects of atomic content and synthesis conditions on catalytic performance are in progress to assess the influence of Pt and Fe in CO-PROX catalysis.

## Declaration of competing interest

The authors declare that they have no known competing financial interests or personal relationships that could have appeared to influence the work reported in this paper.

## Acknowledgments

FAPESP Proc. nos 2017/15469–5, 2019/08051–0, 2015/26308–7, 2014/09087–4, FAPESP/Shell Proc. no 2014/50279–4 (RCGI), FAPESP/Shell Proc. no 2017/11937–4 (CINE) and CNPq Proc. no 304869/2016–3 are grateful for financial support. Centro de Ciência e Tecnologia dos Materiais (CCTM) – IPEN-CNEN/SP are acknowledged for the use of TEM facilities.

## Appendix A. Supplementary data

Supplementary data to this article can be found online at https://doi.org/10.1016/j.ijhydene.2021.02.192.

## REFERENCES

[1] Rahwanto A, Jalil Z, Akhyar Handoko E. Desorption properties of mechanically milled MgH2 with double catalysts Ni and SiC. IOP Conf Ser Mater Sci Eng 2020:931. https://doi.org/10.1088/1757-899X/931/1/012012.

[2] Abe JO, Popoola API, Ajenifuja E, Popoola OM. Hydrogen energy, economy and storage: review and recommendation. Int J Hydrogen Energy 2019;44:15072–86. https://doi.org/10.1016/j.ijhydene.2019.04.068.

[3] Rand DAJ. A journey on the electrochemical road to sustainability. J Solid State Electrochem 2011;15:1579–622. https://doi.org/10.1007/s10008-011-1410-z.

[4] da Silva Veras T, Mozer TS, da Costa Rubim Messeder dos Santos D, da Silva César A. Hydrogen: trends, production and characterization of the main process worldwide. Int J Hydrogen Energy 2017;42:2018–33. https://doi.org/10.1016/j.ijhydene.2016.08.219.

[5] Zegers P. Fuel cell commercialization: the key to a hydrogen economy. J Power Sources 2006;154:497–502. https://doi.org/10.1016/j.jpowsour.2005.10.051.

[6] Staffell I, Scamman D, Velazquez Abad A, Balcombe P, Dodds PE, Ekins P, et al. The role of hydrogen and fuel cells in the global energy system. Energy Environ Sci 2019;12:463–91. https://doi.org/10.1039/c8ee01157e.

[7] El-Emam RS, Özcan H. Comprehensive review on the techno-economics of sustainable large-scale clean hydrogen production. J Clean Prod 2019;220:593–609. https://doi.org/10.1016/j.jclepro.2019.01.309.

[8] Li Q, He R, Gao J-A, Jensen JO, Bjerrum NJ. The CO poisoning effect in PEMFCs operational at temperatures up to 200 C. J Electrochem Soc 2003;150:A1599–605.

[9] Srinivasan S. Fuel cells: from fundamentals to applications. Springer Science & Business media; 2006.

[10] Liu K, Wang A, Zhang T. Recent advances in preferential oxidation of co reaction over platinum group metal catalysts. ACS Catal 2012;2:1165–78. https://doi.org/10.1021/cs200418w.

[11] Chen D, Liu Z, Guo Z, Yan W, Ruan M. Decorating Cu2O photocathode with noble-metal-free Al and NiS cocatalysts for efficient photoelectrochemical water splitting by light harvesting management and charge separation design. Chem Eng J 2020;381:122655. https://doi.org/10.1016/j.cej.2019.122655.

[12] Zhang S, Liu Z, Yan W, Guo Z, Ruan M. Decorating non-noble metal plasmonic Al on a TiO2/Cu2O photoanode to boost performance in photoelectrochemical water splitting. Chin J Catal 2020;41:1884–93. https://doi.org/10.1016/S1872-2067(20)63637-3.

[13] Li Y, Liu Z, Guo Z, Ruan M, Li X, Liu Y. Efficient WO3 photoanode modified by Pt layer and plasmonic Ag for enhanced charge separation and transfer to promote photoelectrochemical performances. ACS Sustainable Chem Eng 2019;7:12582–90. https://doi.org/10.1021/acssuschemeng.9b02450.

[14] Chen D, Liu Z, Guo Z, Yan W, Xin Y. Enhancing light harvesting and charge separation of Cu2O photocathodes with spatially separated noble-metal cocatalysts towards highly efficient water splitting. J Mater Chem 2018;6:20393–401. https://doi.org/10.1039/c8ta07503d.

[15] Ashraf MA, Ercolino G, Specchia S, Specchia V. Final step for CO syngas clean-up: comparison between CO-PROX and CO-SMET processes. Int J Hydrogen Energy 2014;39:18109–19.

[16] Saavedra J, Whittaker T, Chen Z, Pursell CJ, Rioux RM, Chandler BD. Controlling activity and selectivity using water in the Au-catalysed preferential oxidation of CO in H2. Nat Chem 2016;8:584–9. https://doi.org/10.1038/nchem.2494.

[17] Liu Y, Liu B, Liu Y, Wang Q, Hu W, Jing P, et al. Improvement of catalytic performance of preferential oxidation of CO in H2-rich gases on three-dimensionally ordered macro-and meso-porous Pt–Au/CeO2 catalysts. Appl Catal B Environ 2013;142:615–25.

[18] Jardim E de O, Rico-Francés S, Coloma F, Anderson JA, Ramos-Fernandez EV, Silvestre-Albero J, et al. Preferential oxidation of CO in excess of H2 on Pt/CeO2–Nb2O5 catalysts. Appl Catal Gen 2015;492:201–11.

[19] Wootsch A, Descorme C, Duprez D. Preferential oxidation of carbon monoxide in the presence of hydrogen (PROX) over ceria–zirconia and alumina-supported Pt catalysts. J Catal 2004;225:259–66.

[20] Kugai J, Moriya T, Seino S, Nakagawa T, Ohkubo Y, Nitani H, et al. CeO2-supported Pt–Cu alloy nanoparticles synthesized

by radiolytic process for highly selective CO oxidation. Int J Hydrogen Energy 2012;37:4787–97.
[21] Aragao IB, Bueno JMC, Zanchet D. Platinum clusters deposited on maghemite applied to preferential oxidation of CO under hydrogen rich conditions (PROX-CO). Appl Catal Gen 2018;568:86–94. https://doi.org/10.1016/j.apcata.2018.09.014.
[22] Gatla S, Aubert D, Agostini G, Mathon O, Pascarelli S, Lunkenbein T, et al. Room-temperature CO oxidation catalyst: low-temperature metal–support interaction between platinum nanoparticles and nanosized ceria. ACS Catal 2016;6:6151–5.
[23] Lopez A, Larrea A, Sebastian V, Calatayud MP, Irusta S, Santamaria J. Ultrasmall platinum nanoparticles on Fe3O4: a low-temperature catalyst for the preferential oxidation reaction. ChemCatChem 2016;8:1479–84. https://doi.org/10.1002/cctc.201600095.
[24] Hu X, Gao Y, Wang W, Chen C. Structural features and catalytic performance in CO preferential oxidation of MWCNT-supported Pt–Fe catalysts. Int J Hydrogen Energy 2016;41:14079–87.
[25] Zhang H, Liu X, Zhang N, Zheng J, Zheng Y, Li Y, et al. Construction of ultrafine and stable PtFe nano-alloy with ultra-low Pt loading for complete removal of CO in PROX at room temperature. Appl Catal B Environ 2016;180:237–45. https://doi.org/10.1016/j.apcatb.2015.06.032.
[26] Trovarelli A, Llorca J. Ceria catalysts at nanoscale: how do crystal shapes shape catalysis? ACS Catal 2017;7:4716–35. https://doi.org/10.1021/acscatal.7b01246.
[27] Da Silva TL, Da Silva AHM, Assaf JM. Preparation of core-shell Pt@Fe3O4@SiO2 nanostructures by oxidation of core-shell FePt@SiO2 nanoflowers and their performance in preferential CO oxidation reaction. Mater Res Express 2019;6. https://doi.org/10.1088/2053-1591/aae69d.
[28] Kotobuki M, Watanabe A, Uchida H, Yamashita H, Watanabe M. Reaction mechanism of preferential oxidation of carbon monoxide on Pt, Fe, and Pt-Fe/mordenite catalysts. J Catal 2005;236:262–9. https://doi.org/10.1016/j.jcat.2005.09.026.
[29] Tanaka KI, Moro-Oka Y, Ishigure K, Yajima T, Okabe Y, Kato Y, et al. A new catalyst for selective oxidation of CO in H 2 : Part 1, activation by depositing a large amount of FeO x on Pt/Al 2 O 3 and Pt/CeO 2 catalysts. Catal Lett 2004;92:115–21.
[30] Roberts GW, Chin P, Sun X, Spivey JJ. Preferential oxidation of carbon monoxide with Pt/Fe monolithic catalysts: interactions between external transport and the reverse water-gas-shift reaction. Appl Catal B Environ 2003;46:601–11. https://doi.org/10.1016/j.apcatb.2003.07.002.
[31] Kameoka S, Wakabayashi S, Abe E, Tsai AP. One-step synthesis of a high performance Pt-Fe3O4 catalyst: intermetallic Al13Fe4 as a platform and precursor. Catal Lett 2016;146:1309–16. https://doi.org/10.1007/s10562-016-1757-y.
[32] Zhang H, Lin D, Xu G, Zheng J, Zhang N, Li Y, et al. Facile synthesis of carbon supported Pt-nanoparticles with Fe-rich surface: a highly active catalyst for preferential CO oxidation. Int J Hydrogen Energy 2015;40:1742–51. https://doi.org/10.1016/j.ijhydene.2014.12.006.
[33] Dreyer JAH, Grossmann HK, Chen J, Grieb T, Gong BB, Sit PHL, et al. Preferential oxidation of carbon monoxide over Pt-FeOx/CeO2 synthesized by two-nozzle flame spray pyrolysis. J Catal 2015;329:248–61. https://doi.org/10.1016/j.jcat.2015.05.003.
[34] Gosavi PV, Biniwale RB. Catalytic preferential oxidation of carbon monoxide over platinum supported on lanthanum ferriteeceria catalysts for cleaning of hydrogen. J Power Sources 2013;222:1–9. https://doi.org/10.1016/j.jpowsour.2012.07.095.
[35] Fu Q, Li WX, Yao Y, Liu H, Su HY, Ding M, et al. Interface-confined ferrous centers for catalytic oxidation. Science 2010;328:1141–4. https://doi.org/10.1126/science.1188267.
[36] Yin J, Wang J, Zhang T, Wang X. Novel alumina-supported PtFe alloy nanoparticles for preferential oxidation of carbon monoxide in hydrogen. Catal Lett 2008;125:76–82. https://doi.org/10.1007/s10562-008-9513-6.
[37] Siani A, Captain B, Alexeev OS, Stafyla E, Hungria AB, Midgley PA, et al. Improved CO oxidation activity in the presence and absence of hydrogen over cluster-derived PtFe/SiO 2 catalysts. Langmuir 2006;22:5160–7. https://doi.org/10.1021/la053476a.
[38] Tanaka KI, Shou M, He H, Shi X. Significant enhancement of the oxidation of CO by H2 and/or H2O on a FeO x/Pt/TiO2 catalyst. Catal Lett 2006;110:185–90. https://doi.org/10.1007/s10562-006-0107-x.
[39] Cao L, Liu W, Luo Q, Yin R, Wang B, Weissenrieder J, et al. Atomically dispersed iron hydroxide anchored on Pt for preferential oxidation of CO in H2. Nature 2019;565:631–5. https://doi.org/10.1038/s41586-018-0869-5.
[40] Lou Y, Liu J. A highly active Pt-Fe/γ-Al2O3 catalyst for preferential oxidation of CO in excess of H2 with a wide operation temperature window. Chem Commun 2017;53:9020–3. https://doi.org/10.1039/c7cc03787b.
[41] Watanabe M, Uchida H, Ohkubo K, Igarashi H. Hydrogen purification for fuel cells: selective oxidation of carbon monoxide on Pt-Fe/zeolite catalysts. Appl Catal B Environ 2003;46:595–600. https://doi.org/10.1016/S0926-3373(03)00322-9.
[42] Ma HC, Xue XZ, Liao JH, Liu CP, Xing W. Effect of borohydride as reducing agent on the structures and electrochemical properties of Pt/C catalyst. Appl Surf Sci 2006;252:8593–7. https://doi.org/10.1016/j.apsusc.2005.11.089.
[43] Alencar CSL, Paiva ARN, Da Silva JCM, Vaz JM, Spinace EV. One-step synthesis of AuCu/TiO2catalysts for CO preferential oxidation. Mater Res 2020;23:2–7. https://doi.org/10.1590/1980-5373-MR-2020-0181.
[44] Leal GB, Ciotti L, Watacabe BN, Loureiro da Silva DC, Antoniassi RM, Silva JCM, et al. Preparation of Au/TiO2 by a facile method at room temperature for the CO preferential oxidation reaction. Catal Commun 2018;116:38–42. https://doi.org/10.1016/j.catcom.2018.07.021.
[45] de Souza Pereira JM, Ciotti L, Vaz JM, Spinace EV. Preparation of Au/TiO2 catalyst by a liquid-phase reduction method for preferential oxidation of carbon monoxide in a hydrogen rich-stream (CO-PROX reaction). Mater Res 2018;21:1–6. https://doi.org/10.1590/1980-5373-MR-2017-0756.
[46] Yadav R, Singh H, Sinha AK. Ultra-fine size-controlled Pt (111) nanoparticles supported on mesoporous titania as an efficient photoelectrocatalyst for hydrogen evolution. Appl Surf Sci 2019;495:143525. https://doi.org/10.1016/j.apsusc.2019.07.267.
[47] Harrison BB, Diwell AF, Hallett C. Promoting platinum metals by ceria - metal-support interactions in autocatalysts. Platin Met Rev 1988:73–83.
[48] Ivanov I, Petrova P, Georgiev V, Batakliev T, Karakirova Y, Serga V, et al. Comparative study of ceria supported nano-sized platinum catalysts synthesized by extractive-pyrolytic method for Low-Temperature WGS reaction. Catal Lett 2013;143:942–9. https://doi.org/10.1007/s10562-013-1078-3.
[49] Queiroz CMS, Machado AP, Paiva ARN, Antoniassi RM, Vaz JM, Spinacé EV. Active Pt/CeO2 catalysts prepared by an alcohol-reduction process for low-temperature CO-PROX reaction. Mater Renew Sustain Energy 2019;8:1–8. https://doi.org/10.1007/s40243-019-0155-y.
[50] Carvalho DR, Aragao IB, Zanchet D. Pt-CeO 2 catalysts synthesized by glucose assisted hydrothermal method: impact of calcination parameters on the structural

properties and catalytic performance in PROX-CO. J Nanosci Nanotechnol 2017;18:3405–12. https://doi.org/10.1166/jnn.2018.14659.

[51] Rico-Francés S, Jardim E de O, Wezendonk TA, Kapteijn F, Gascon J, Sepúlveda-Escribano A, et al. Highly dispersed Ptδ+ on TixCe (1–x) O2 as an active phase in preferential oxidation of CO. Appl Catal B Environ 2016;180:169–78.

[52] Khobragade R, Yearwar D, Labhsetwar N, Saravanan G. Alumina supported nano-platinum on copper nanoparticles prepared via galvanic displacement reaction for preferential carbon monoxide oxidation in presence of hydrogen. Int J Hydrogen Energy 2019;44:28757–68.

[53] Gänzler AM, Casapu M, Maurer F, Störmer H, Gerthsen D, Ferré G, et al. Tuning the Pt/CeO2 interface by in situ variation of the Pt particle size. ACS Catal 2018;8:4800–11. https://doi.org/10.1021/acscatal.8b00330.

[54] Song S, Wu Y, Ge S, Wang L, Wang Y, Guo Y, et al. A facile way to improve Pt atom efficiency for CO oxidation at low temperature: modification by transition metal oxides. ACS Catal 2019;9:6177–87. https://doi.org/10.1021/acscatal.9b01679.

[55] Potemkin DI, Saparbaev ES, Zadesenets AV, Filatov EY, Snytnikov PV, Sobyanin VA. Preferential CO oxidation on bimetallic Pt0.5M0.5 catalysts (M = Fe, Co, Ni) prepared from double complex salts. Catalogue Index 2018;10:62–7. https://doi.org/10.1134/S2070050418010099.

[56] Ro I, Aragao IB, Chada JP, Liu Y, Rivera-Dones KR, Ball MR, et al. The role of Pt-FexOy interfacial sites for CO oxidation. J Catal 2018;358:19–26. https://doi.org/10.1016/j.jcat.2017.11.021.